Nitrogen-doped carbon dots derived from polyvinyl pyrrolidone and their multicolor cell imaging

Nitrogen-doped carbon dots derived from polyvinyl pyrrolidone and their multicolor cell imaging

Hui Ding[1], Peng Zhang[1], Tian-Yi Wang[1], Ji-Lie Kong[1,2] and Huan-Ming Xiong[1]

[1] Department of Chemistry, Fudan University, Shanghai 200433, People's Republic of China
[2] Institutes of Biomedical Sciences, Fudan University, Shanghai 200032, People's Republic of China

E-mail: jlkong@fudan.edu.cn and hmxiong@fudan.edu.cn

Abstract

Nitrogen-doped carbon dots (N-CDs) with a high quantum yield of 19.6% were prepared by calcining polyvinyl pyrrolidone (PVP, K-30), and then modified with 4,7,10-trioxa-1,13-tridecanediamine. The as-prepared N-CDs exhibited excitation-dependent and pH-sensitive photoluminescence. Transmission electron microscopy and Raman spectra demonstrated the graphitic structure of the N-CDs. Fourier transform infrared spectroscopy and x-ray diffraction studies revealed successful passivation and the presence of hydrophilic groups on the surface. Importantly, such modified quantum dots acted as good multicolor cell imaging probes due to their excellent fluorescent properties, low cytotoxicity and fine dispersity.

S Online supplementary data available from stacks.iop.org/NANO/25/205604/mmedia

Keywords: carbon dots, photoluminescence, bioimaging, doping, cytotoxicity

(Some figures may appear in colour only in the online journal)

1. Introduction

Luminescent semiconductor quantum dots have attracted a great deal of attention due to their unique optical properties and promising biological applications [1, 2]. However, typical semiconductor quantum dots contain heavy metals as necessary elements, which results in them having poor biocompatibility with biological cells or tissue [3]. Hence, developing nontoxic and multicolor luminescent, especially red-emitting, nanoparticles for optical imaging applications is important in this area. Since photoluminescent carbon dots (CDs) were first obtained in 2004 [4], they have been considered as new candidates for better biological application due to their unique physical properties, good biocompatibility and low toxicity [5–7]. Carbon dots generally consist of three common elements: carbon, hydrogen and oxygen. In recent years, doped carbon dots have been a subject of topical interest in carbon material research because of their excellent

performance in catalysis, bioimaging and sensing [8–11]. It was reported that heteroatoms doped in carbon dots, such as nitrogen, played a vital role in tuning the fluorescence emission of carbon dots and introduced some new surface states [11–13]. To date, the synthetic conditions of N-doped carbon dots (N-CDs) are similar to those of carbon dots, including reflux, microwaves, ultrasonication, hydrothermal treatment and calcination [8, 12, 14, 15]. For example, Zhang's group [11] synthesized nitrogen-doped carbon dots by solvothermal treatment on CCl_4 and $NaNH_2$, which were used as fluorescent probes for cell imaging. Li et al [16] prepared N-CDs by applying hydrothermal treatments onto natural substances such as silk for the detection of Fe^{3+}. Huang et al [17] synthesized N-CDs through the hydrothermal carbonization of strawberry juice for the detection of Hg^{2+}. Zhu and coworkers [18] fabricated N-CDs by hydrothermal treatment on soya milk, which were used as electrocatalysts for oxygen reduction. Ma et al [8] adopted glucose and aqua ammonia to

synthesize N-CDs for the photodegradation of methyl orange (MO) under visible light. However, these successful results also had some disadvantages, such as producing toxic volatile by-products [11], costing too much in terms of reaction time [16] or producing N-CDs with very low quantum yield [8, 17, 18].

In this research, we present a facile and rapid route to prepare nitrogen-doped carbon dots (N-CDs) by pyrolysis of a new precursor PVP at 400 °C. After passivation with 10-trioxa-1,13-tridecanediamine (TTDDA), the quantum yield (QY) of the as-prepared N-CD-TTDDAs was improved from 6.4% to 19.3% at the maximum emission. These N-CDs exhibit good dispersion in water, excellent fluorescent stability and low toxicity, especially the multicolor imaging function in the living cells.

2. Materials and methods

2.1. Materials

Polyvinyl pyrrolidone (K-30) and ethanol were purchased from Sinopharm Chemical Reagent Co. Ltd. 4-, 7- and 10-trioxa-1,13-tridecanediamine (TTDDA) was purchased from Fluka. All chemicals were used as received without any further purification. Ultrapure water (Milli-Q water) was used in all experiments.

2.2. Synthesis of the modified N-CDs

1.0 g of polyvinyl pyrrolidone (K-30) was placed in a quartz boat inside a tube furnace. The temperature was increased to 400 °C within 100 min and the sample was annealed at this temperature for 3 h, and cooled to ambient temperature naturally. The whole process was carried out in an air atmosphere. The obtained black product was ground into a fine powder and put into 30 mL of ethanol. The mixture was sonicated for 1 h. After that, the mixture was centrifuged with 150 00 rpm for 15 min to remove large-sized particles. The light-yellow supernatant was collected and evaporated to remove ethanol. After that, the product was dispersed into 20 mL of ultrapure water. 20 mL of N-CD solution and 0.5 g of TTDDA were mixed in a polytetrafluorethylene-lined stainless steel autoclave. The mixture was heated at 170 °C for 12 h. Then, the N-CD solution was purified via dialysis through an analysis membrane (Spectrum, MW cutoff 3500) for 3 days. Finally, a homogeneous light-yellow and photoluminescent N-CD solution was obtained. The N-doped carbon dot aqueous solution was freeze-dried for characterization.

2.3. Characterization

A JEM-2010 transmission electron microscope operating at 200 kV was employed to obtain high resolution transmission electron microscopy (HRTEM) images. The Raman spectrum of the as-prepared samples was recorded by a LabRam-1B microRaman spectrometer (excitation wavelength: 638.2 nm). Fourier transform infrared (FTIR) spectra were recorded on a Nicolet Nexus 470 FTIR spectrometer. The UV-Vis absorption spectra were recorded on a Unico UV-2802 PC spectrometer. The photoluminescence (PL) spectra were measured by a Horiba JobinYvon fluoromax-4 spectrofluorometer equipped with a HORIBF-3004 sample heater/cooler Peltierthermocouple drive and an F-3018 quantum yield accessory including an integrating sphere. The surface species were detected by x-ray photoelectron spectroscopy (XPS) using a Perkin Elmer PHI5000C. The dynamic light scattering (DLS) spectra were measured at 25 °C on a Zetasizer instrument (ZS-90, Malvern). The time-resolved fluorospectroscopy of the sample was measured by a fluorescence lifetime spectrometer (QM 40, PTI). The crystal structure of the N-CDs was characterized by a Bruker D8 Advance x-ray diffractometer ($\lambda = 0.154\,056$ nm).

2.4. Photostability tests

A photostability comparison between a N-CD solution and a rhodamine-6G solution with optical densities below 0.1 was conducted by continuous irradiation under a UV lamp and laser. After irradiation for different lengths of time, the fluorescent intensity of the samples was measured on the fluorescence spectrometer under the same conditions.

2.5. Cell viability assay

HeLa cells were seeded in a 96-well cell culture plate in Dulbecco's modified Eagle medium (DMEM) at a density of 5×10^4 cells per mL with 10% fetal bovine serum (FBS) at 37 °C and with 5% CO_2 for 24 h. Afterwards, the culture medium was replaced with 200 μL of DMEM containing the carbon dots at different doses and cultured for another 48 h. Then, 20 μL of 5 mg mL^{-1} MTT (3-(4,5-dimethylthiazol-2yl)-2,5-diphenyltetrazolium bromide) solution was added to every cell well. The cells were further incubated for 4 h, followed by removing the culture medium with MTT, and then 150 μL of DMSO was added. The resulting mixture was shaken for 15 min at room temperature. The absorbance of MTT at 492 nm was measured by an automatic ELISA analyzer (SPR-960). The control data was obtained in the absence of N-CDs. Each experiment was performed 5 times and the average data was presented.

2.6. Cell imaging experiments

Cellular fluorescent images were recorded on a Leica Tcs sp5 Laser Scanning Confocal Microscope. HeLa cells were seeded in 6-well culture plates at a density of 10^5 per well in DMEM containing 10% fetal bovine serum (FBS) at 37 °C in a 5% CO_2 incubator for 24 h. Then, the mixture of N-CDs (0.1 mg mL^{-1}) in the DMEM medium was added into each well. After 3 h of incubation in 5% CO_2 at 37 , the cells were washed twice with phosphate buffer solution (PBS) to remove extracellular N-CDs and were then fixed with 4% paraformaldehyde.
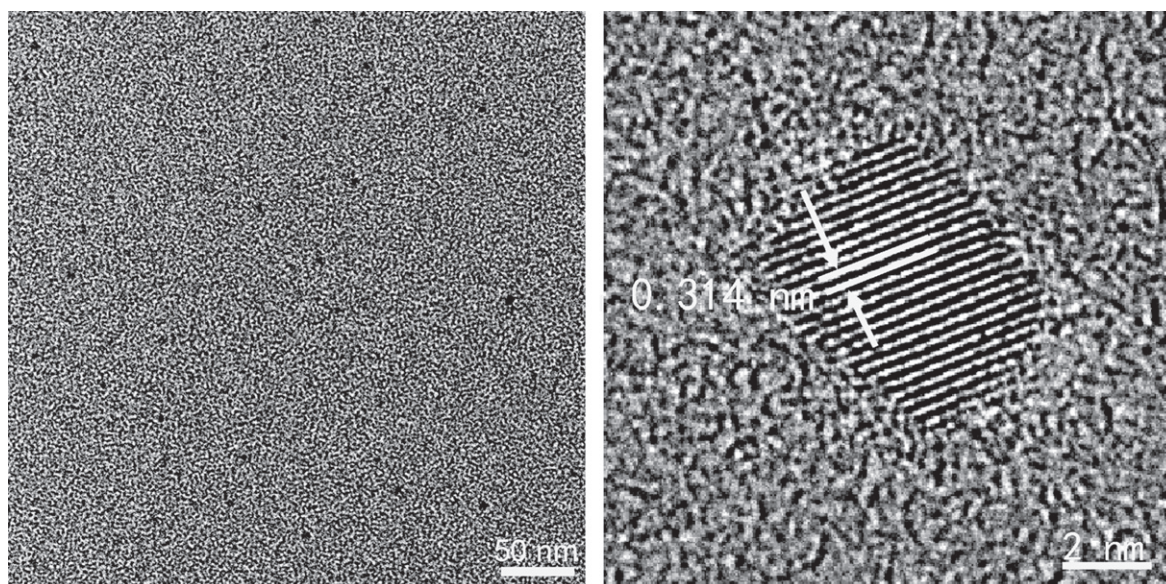
Scheme 1. Synthetic route of the passivated N-CDs from PVP (K-30).

2.7. Quantum yield measurement

Quantum yield was measured on an integrating sphere attached to a Horiba Jobin Yvon fluoromax-4 spectro-fluorometer. Firstly, the aqueous solution of the carbon dots was diluted to keep absorption intensity under 0.1 at the excitation wavelength (370 nm) in the 10 mm fluorescence cuvette. Subsequently, the sample was placed in the integrating sphere and excited by monochromatic light of 370 nm. We recorded the fluorescent spectrum of our sample from 360–380 nm and 385–720 nm, respectively. Meanwhile, we also recorded the same fluorescence spectrum of the pure water under the same conditions. Finally, we used the fluorescent software to calculate the quantum yield. Each experiment was conducted three times in parallel and the average value of the quantum yield was presented. In this paper, we also tested the quantum yield of green and red emission of the nitrogen-doped carbon dots. The excitation wavelengths were 458 nm and 514 nm, respectively. The corresponding fluorescence data was recorded from 448–468 nm and 490–570 nm when excited by 458 nm. The other fluorescence spectrum was collected from 504–524 nm and 575–720 nm when excited by 514 nm.

The detailed principles of the integrating sphere are described below. When a sample is placed in the integrating sphere and excited with monochromatic light of wavelength λ, the film absorbance, A, is calculated by

$$A = \frac{L_b - L_c}{L_b} \qquad (1)$$

where L_b is the integrated excitation profile when the sample is diffusely illuminated by the integrating sphere's surface and L_c is the integrated excitation profile when the sample is directly excited by the incident beam.

The quantum yield, Φ, by definition represents photons emitted to photons absorbed:

$$\Phi = \frac{E_c - (1 - A) \cdot E_b}{L_a \cdot A} = \frac{E_c - E_a}{L_a - L_c} \qquad (2)$$

where E_c is the integrated luminescence of the film caused by direct excitation and E_b is the integrated luminescence of the film caused by indirect illumination from the sphere. The term L_a is the integrated excitation profile from an empty integrating sphere (without the sample, only a blank). Here E_a is the integrated luminescence from an empty integrating sphere (only a blank).

For integration of the function L over the wavelength λ, the integration limits can range from 10 nm below the excitation wavelength to 10 nm above the excitation wavelength.

3. Results and discussion

The preparation procedure for N-CD-TTDDAs from polyvinyl pyrrolidone is illustrated in scheme 1. Polyvinyl pyrrolidone was carbonized with a tube furnace then ground into powder. The mixture of powder and ethanol was placed under ultrasonic processing to extract N-CDs. After evaporating the ethanol, the CDs were passivated by TTDDA to increase the quantum yield. The pale-yellow solution containing N-CD-TTDDAs was obtained after dialysis.

3.1. Structural analyses

The TEM image in figure 1 (left) shows that the N-CD-TTDDA nanoparticles are uniform and monodispersed, with an average diameter of about 4 nm (figure S1, available at stacks.iop.org/NANO/25/205604/mmedia). Their hydrodynamic diameters, measured by dynamic light scattering (figure S2) are about 5 nm (PDI < 0.304), which confirms the observation results by TEM. The HRTEM (right) results present the average lattice spaces of these N-CDs as 0.314 nm, corresponding to the (002) planes of graphite [19–22]. X-ray diffraction was also used to characterize the prepared N-CDs (figure S3). The pattern has a diffraction peak at 25.4°, indicating that the interlayer spacing is about 0.34 nm, similar to the above HRTEM result.

The Raman spectrum of the modified N-CDs in figure 2(D) reveals that our product possesses two peaks. One, at 1369 cm^{-1}, assigned to the D band (sp^3), is associated with the vibration of carbon atoms with dangling bonds in the termination plane of disordered carbon. The other, at 1590 cm^{-1}, assigned to the G band (sp^2), represents the E$_{2g}$ mode of graphite that is the sp^2 vibration of carbon in a two-dimensional hexagonal lattice. The intensity ratio of the D and G bands (I$_D$/I$_G$) is 0.441, implying that the unsaturated carbon is primarily in the N-doped carbon dots [6].

The FTIR technique was used to identify the organic functional groups on the surface of the modified N-CDs. As shown in figure 2(C), the amide group is clearly identified both through the 1661 cm^{-1} C=O stretching vibration and the 1291 cm^{-1} C–N. Both samples have absorptions at 3400 cm^{-1} and 1100 cm^{-1}, which are ascribed to N-H asymmetric stretching vibration and C–O stretching vibrations, respectively [7]. The absorption peak of C–O and N–H in N-CDs confirms that TTDDA have been successfully grafted to the N-CDs after passivation. The absorption peaks between 2800 cm^{-1} and 3000 cm^{-1} are attributed to the C–H stretching vibration. In addition, the peaks within the range 1300–1500 cm^{-1} represent the C–H bending vibration.

The N-CDs without TTDDA passivation were studied by x-ray photoelectron spectroscopy (XPS) to verify the doping state of the nitrogen element in the nanoparticles

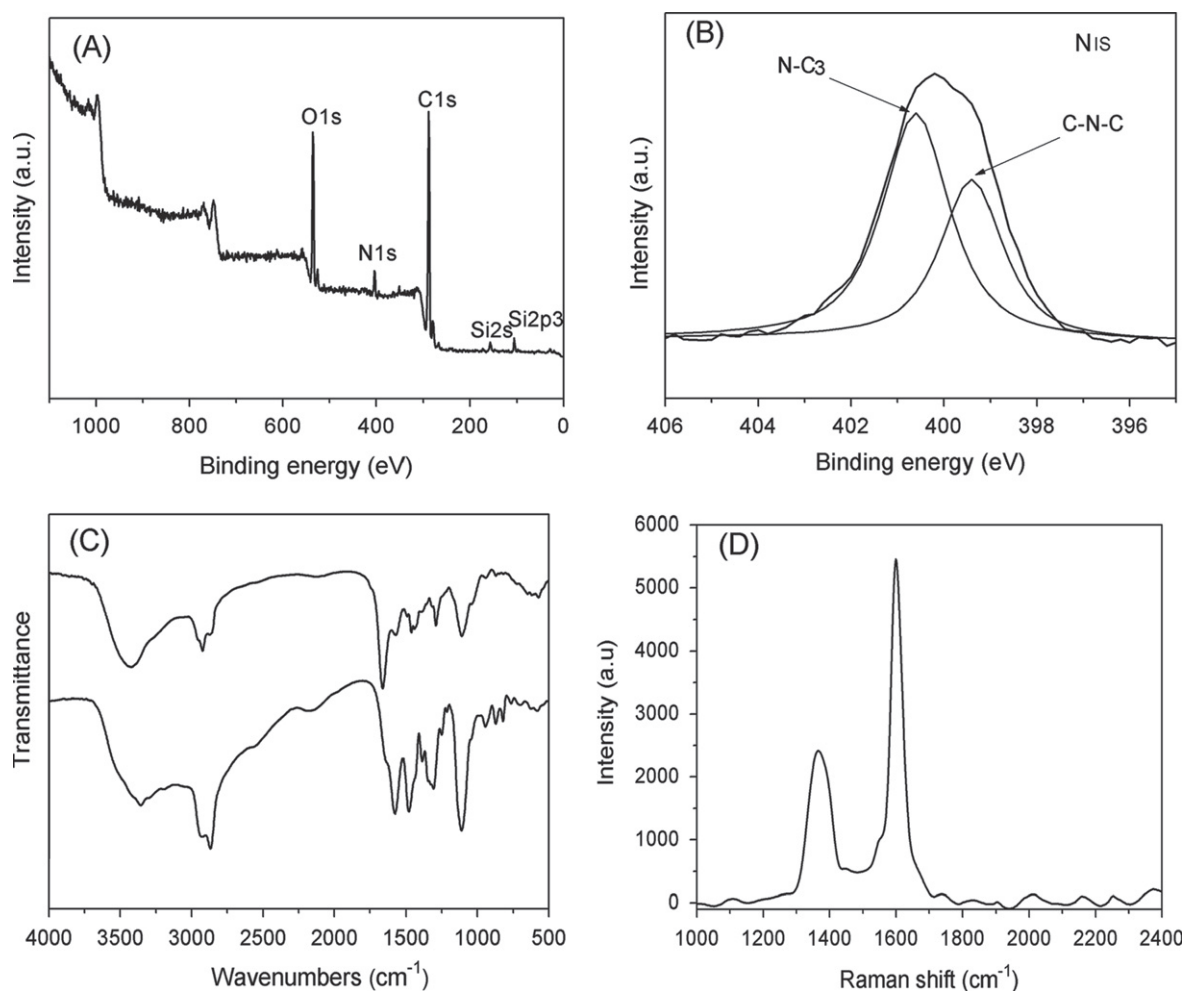**Figure 1.** TEM (left) and HRTEM (right) images of N-CD-TTDDAs.

Figure 2. (A) XPS analyses of the crude N-CD nanoparticles. (B) The N_{1s} band of the same sample. (C) FTIR spectra of the N-CDs passivated with TTDDA (upper line) and TTDDA itself (lower line). (D) Raman spectrum of the N-CD-TTDDAs.

(figure 2(A)). Three bands at around 284.5, 400.0 and 531.0 eV, representing C_{1s}, N_{1s} and O_{1s}, respectively [16], are observed in the survey spectra of N-CDs, while the Si_{2s} and Si_{2p} peaks result from the glass substrate. After deconvolution
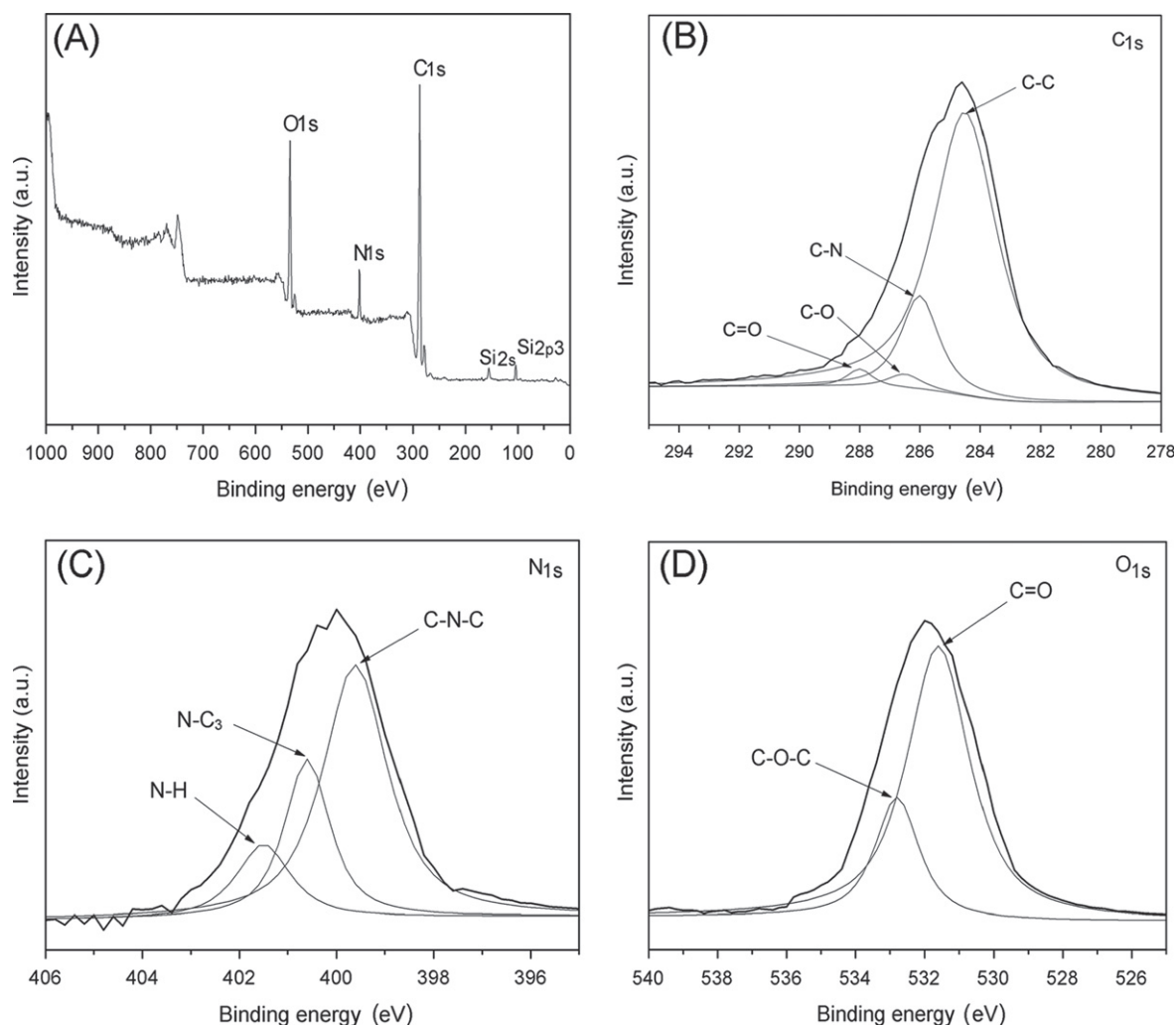
Figure 3. XPS spectra of the N-CD-TTDDAs. (A) Survey spectrum of the N-CD-TTDDAs, and the corresponding (B) C_{1s} spectrum, (C) N_{1s} spectrum and (D) O_{1s} spectrum of the N-CD-TTDDAs.

of the N_{1s} band (figure 2(B)), the XPS peaks at 400.6 and 399.4 eV are assigned to N–C_3 and C–N–C respectively, confirming that the nitrogen element has been doped into the CDs in the pyrolysis. Meanwhile, we also studied the XPS of the passivated N-CDs. The survey spectrum of the N-CD-TTDDAs (figure 3(A)) reveals three typical peaks of C_{1S}, N_{1S} and O_{1S}. The high resolution scan of the C_{1S} spectrum (figure 3(B)) can be deconvoluted into four peaks at 284.5 (C–C), 286.0 (C–N), 286.7 (C–O), and 288.0 (C=O) eV, which are consistent with the FTIR results. Meanwhile, the N_{1s} spectrum (figure 3(C)) shows the presence of nitrogen in three chemical environments, corresponding to 399.4 (C–N–C), 400.6 (N–C_3) and 401.5 (N–H) eV. Moreover, the spectrum of O_{1S} (figure 3(D)) also shows two relative oxygen species of 531.6 (C=O), and 533.1 (C–O–C) eV [16]. The existence of C–O–C and a new peak representing N–H can further confirm that passivation has been successfully completed, in accordance with the FTIR analyses. After modification with TTDDA, the nitrogen composition increases from 4.80% to 6.92% (table S1), which is ascribed to the higher nitrogen element in the TTDDA (12.71%).
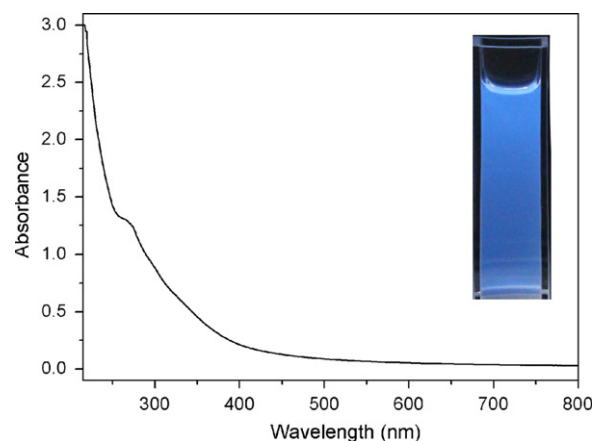
Figure 4. UV-Vis absorption spectra of the N-CD-TTDDAs in water. The inset picture is the sample under a UV lamp (the excitation wavelength is 360 nm).

3.2. Optical properties

Figure 4 shows the UV-Vis absorption curve of the as-prepared N-CD-TTDDAs and the inset photo of our N-CD-
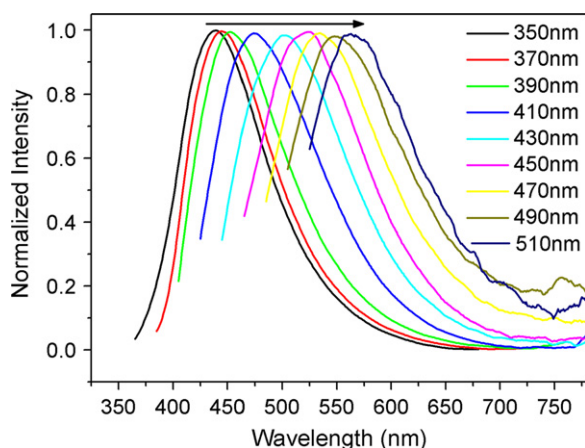
Figure 5. Normalized photoluminescent emission spectra of the N-CD-TTDDAs in water obtained by excitation of different wavelengths, respectively.

Figure 6. The time-resolved photoluminescence decay profiles of N-CD-TTDDAs (monitored at 450 nm, λ_{ex} = 368 nm).

Figure 7. Cytotoxicity of the N-CD-TTDDAs toward HeLa cells from an MTT assay.

TTDDA solution under UV light. A clear adsorption feature is visible at about 270 nm, which is ascribed to the p–p* transition of nanocarbon [18]. Besides, the N-CD-TTDDA sample has a wide absorption band with decreasing intensity, which is the typical character of CDs and is similar to other reports [16, 18]. Such a wide absorption band ensures the photoluminescent emission of the N-CD-TTDDAs under excitation from UV light to red light. A considerable absorption coefficient of CDs in the visible region is very important for exciting red/NIR fluorescence under confocal laser scanning microscopy (CLSM) observation. Many CDs failed to emit red fluorescence with enough intensity under CLSM because their absorption in the green/yellow region was too weak, as in the case of the nanoparticles derived from 1,2-ethylenediamine (EDA) [14], poly (ethylene glycol) [23] and ethylenediamine-tetraacetic acid (EDTA) salt [24] and urea [25]. Some other CDs derived from cocoon silk [16], citric acid [26] and glycerol [27], could emit weak red fluorescence but they required excitation of violet light which was not preferable for imaging cells and tissues.

Figures 5 and S4 show the typical photoluminescent emission spectra of CDs. Since the band structures of CDs are complicated and disordered, the emission spectra of CDs are usually broad, ranging from the UV to red region, and dependent on the excitation light wavelengths. Our N-CD-TTDDAs show the strongest blue fluorescence under the excitation wavelength of 370 nm, with the highest QY of 19.3% using an integrating sphere for accurate QY evaluation [7], while the green fluorescence with QY of 9.1% and red fluorescence with QY of 4.2% are obtained by excitation wavelengths of 458 nm and 514 nm, respectively. The time-resolved PL decay profiles of N-CDs with excitation wavelengths of 368 nm are shown in figure 6. The corresponding lifetimes, calculated by fitting to exponential functions using iterative reconvolution, are listed in table S2. The obtained τ_1 (10.44 ns) are close to those of the nitrogen-doped carbon dots [10, 13, 15] and longer than those of the carbon dots previously reported [10, 23, 27–29]. It was reported that doping of the nitrogen element might move down the
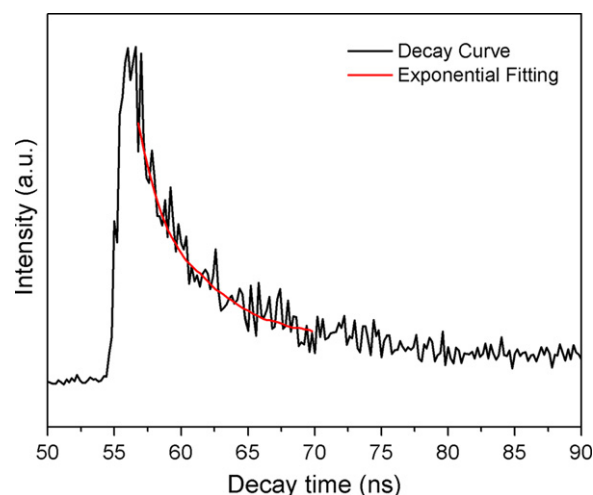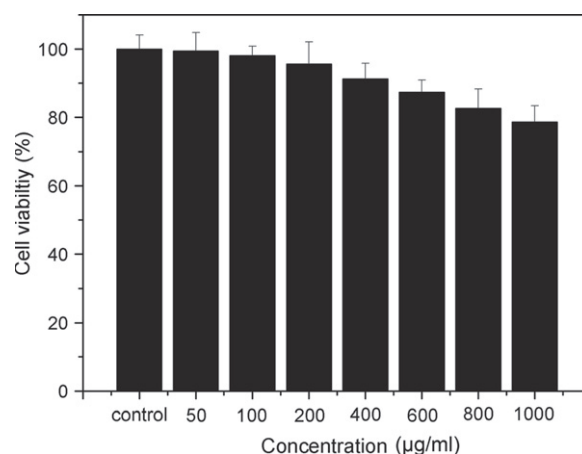
conduction band edge of carbon so as to decrease the band gap, and as a result, the red fluorescence could be excited by green or yellow light. Moreover, the nitrogen bonding to carbon may cause disorder in the carbon hexagonal rings and create new luminescent centers by trapping the radiative electron–hole pairs, so that the QY of the CDs will be improved after doping nitrogen [12, 30–32]. However, the photoluminescent mechanism of CDs remains unclear thus far, so the exact effects of doping nitrogen require deeper exploration in the future.

3.3. Fluorescence stability

The luminescent stability of the N-CD-TTDDAs was tested under different conditions, such as continuous UV and laser irradiation, controlling pH values and changing the ionic strength of the solutions. From figure S6, the fluorescence intensity of the N-CDs exhibited almost no change, while an obvious fluorescent decay was observed for R6G after 2 h of continuous UV irradiation. Meanwhile, we also tested the photostability of red emission of N-CDs (figure S7), and
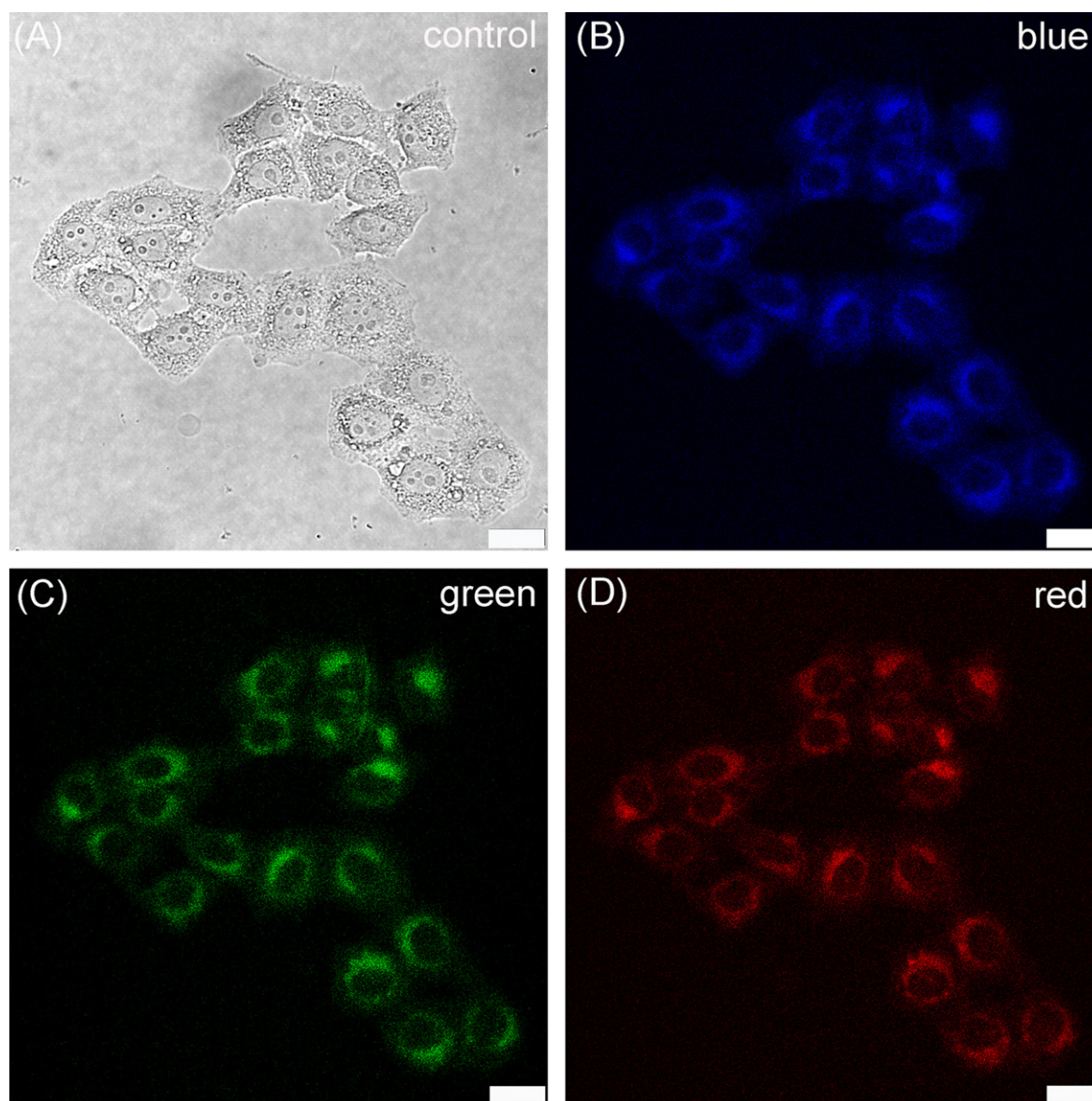
Figure 8. Confocal fluorescence images of HeLa cells after incubation with N-CD-TTDDAs (0.1 mg mL^{-1}) for 3 h: (A) under bright field, (B) under 405 nm excitation and emission recorded at 420–540 nm, (C) under 458 nm excitation and emission recorded at 500–575 nm, (D) under 514 nm excitation and emission recorded at 580–650 nm. All scale bars are 25 μm.

found that the fluorescence intensity experienced almost no change, which makes it very suitable for biological application. Hence, our N-CDs are more stable than conventional dyes for cell imaging. An interesting phenomenon concerning the pH-dependent PL behavior is shown in figure S8. From the results, we can see that PL intensities decrease in a solution of high or low pH, but remain constant in a solution of pH 5–9, which is ascribed to the change of charge density on the surface. Besides, figure S9 reveals that the PL intensities of our N-CDs are very stable at different ionic strengths, which is critical for practical biological application.

3.4. Cytotoxicity tests and cell imaging

Low cytotoxicity is one of the most critical requirements for ideal multifunctional biomaterials with bioimaging capacity.

Hence, cytotoxicity towards HeLa cells was also carried out through the conventional MTT assays (figure 7). After 48 h incubation with N-CD-TTDDA nanoparticles at a practical concentration of 0.1 mg mL^{-1}, HeLa cells had viability over 95%. Even when the concentration was up to 1 mg mL^{-1}, the cells retaining viability represented about 80%, indicating that the N-CD-TTDDAs presented very low cytotoxicity. Thus we could safely use N-CD-TTDDAs of 0.1 mg mL^{-1} for incubation with HeLa cells in Dulbecco's modified medium (DMEM) at 37 °C with 5% CO_2. After 3 h, the cells were brightly illuminated with multicolor fluorescence under different laser pulses of CLSM (figure 8). It was clear that the nanoparticles were located in the cytoplasm while the nuclei were not luminescent. This result confirms that our N-CD-TTDDAs are able to serve as multicolor cell imaging probes.

4. Conclusion

In summary, we synthesized nitrogen-doped carbon dots through calcining cheap and accessible PVP (K-30) in air for the first time and then passivating the product with TTDDA. The as-prepared nanoparticles were monodispersed in water and they showed excellent fluorescent stability, tunable fluorescent emission, low cytotoxicity and considerable fluorescence quantum yield in the red light region. We could thus successfully use such CDs as fluorescent probes for multicolor cell imaging. The present work reveals that nitrogen-doping is an effective method to improve the luminescent properties of CDs, especially to obtain the satisfying red emission of CDs under CLSM imaging.

References

[1] Michalet X, Pinaud F F, Bentolila L A, Tsay J M, Doose S, Li J J, Sundaresan G, Wu A M, Gambhir S S and Weiss S 2005 Quantum dots for live cells, *in vivo* imaging, and diagnostics *Science* **307** 538–44

[2] Jung J, Solanki A, Memoli K A, Kamei K-i, Kim H, Drahl M A, Williams L J, Tseng H-R and Lee K 2010 Selective inhibition of human brain tumor cells through multifunctional quantum-dot-based sirna delivery *Angew. Chem. In. Edn.* **49** 103–7

[3] Derfus A M, Chan W C W and Bhatia S N 2004 Probing the cytotoxicity of semiconductor quantum dots *Nano Lett.* **4** 11–8

[4] Xu X Y, Ray R, Gu Y L, Ploehn H J, Gearheart L, Raker K and Scrivens W A 2004 Electrophoretic analysis and purification of fluorescent single-walled carbon nanotube fragments *J. Am. Chem. Soc.* **126** 12736–7

[5] Baker S N and Baker G A 2010 Luminescent carbon nanodots: emergent nanolights *Angew.Chem. In. Edn.* **49** 6726–44

[6] Li H, Kang Z, Liu Y and Lee S-T 2012 Carbon nanodots: synthesis, properties and applications *J. Mater. Chem.* **22** 24230–53

[7] Ding H, Cheng L W, Ma Y Y, Kong J L and Xiong H M 2013 Luminescent carbon quantum dots and their application in cell imaging *New J. Chem.* **37** 2515–20

[8] Ma Z, Ming H, Huang H, Liu Y and Kang Z 2012 One-step ultrasonic synthesis of fluorescent N-doped carbon dots from glucose and their visible-light sensitive photocatalytic ability *New J. Chem.* **36** 861–4

[9] Lai T, Zheng E, Chen L, Wang X, Kong L, You C, Ruan Y and Weng X 2013 Hybrid carbon source for producing nitrogen-doped polymer nanodots: one-pot hydrothermal synthesis, fluorescence enhancement and highly selective detection of Fe(III) *Nanoscale* **5** 8015–21

[10] Qian Z, Ma J, Shan X, Feng H, Shao L and Chen J 2014 Highly luminescent n-doped carbon quantum dots as an effective multifunctional fluorescence sensing platform *Chem. Eur. J.* **20** 2254–63

[11] Zhang Y Q, Ma D K, Zhuang Y, Zhang X, Chen W, Hong L L, Yan Q X, Yu K and Huang S M 2012 One-pot synthesis of N-doped carbon dots with tunable luminescence properties *J. Mater. Chem.* **22** 16714–8

[12] Xu Y, Wu M, Liu Y, Feng X Z, Yin X B, He X W and Zhang Y K 2013 Nitrogen-doped carbon dots: a facile and general preparation method, photoluminescence investigation, and imaging applications *Chem. Eur. J.* **19** 2276–83

[13] Dong Y, Pang H, Yang H B, Guo C, Shao J, Chi Y, Li C M and Yu T 2013 Carbon-based dots Co-doped with nitrogen and sulfur for high quantum yield and excitation-independent emission *Angew.Chem. In. Edn* **52** 7800–4

[14] Liu S, Tian J, Wang L, Luo Y, Zhai J and Sun X 2011 Preparation of photoluminescent carbon nitride dots from CCl4 and 1,2-ethylenediamine: a heat-treatment-based strategy *J. Mater. Chem.* **21** 11726–9

[15] Yang Z, Xu M, Liu Y, He F, Gao F, Su Y, Wei H and Zhang Y 2014 Nitrogen-doped, carbon-rich, highly photoluminescent carbon dots from ammonium citrate *Nanoscale* **6** 1890–5

[16] Li W, Zhang Z, Kong B, Feng S, Wang J, Wang L, Yang J, Zhang F, Wu P and Zhao D 2013 Simple and green synthesis of nitrogen-doped photoluminescent carbonaceous nanospheres for bioimaging *Angew. Chem. Int. Edn.* **52** 8151–5

[17] Huang H, Lv J J, Zhou D L, Bao N, Xu Y, Wang A J and Feng J J 2013 One-pot green synthesis of nitrogen-doped carbon nanoparticles as fluorescent probes for mercury ions *RSC Adv.* **3** 21691–6

[18] Zhu C, Zhai J and Dong S 2012 Bifunctional fluorescent carbon nanodots: green synthesis via soy milk and application as metal-free electrocatalysts for oxygen reduction *Chem. Commun.* **48** 9367–9

[19] Li H, He X, Kang Z, Huang H, Liu Y, Liu J, Lian S, Tsang C H A, Yang X and Lee S-T 2010 Water-soluble fluorescent carbon quantum dots and photocatalyst design *Angew. Chem. Int. Ed.* **49** 4430–4

[20] Li H, Liu R, Kong W, Liu J, Liu Y, Zhou L, Zhang X, Lee S-T and Kang Z 2014 Carbon quantum dots with photo-generated proton property as efficient visible light controlled acid catalyst *Nanoscale* **6** 867–73

[21] Liu S, Tian J, Wang L, Zhang Y, Luo Y, Asiri A M, Al-Youbi A O and Sun X 2012 A novel acid-driven, microwave-assisted, one-pot strategy toward rapid production of graphitic N-doped carbon nanoparticles-decorated carbon flakes from N,N-dimethylformamide and their application in removal of dye from water *RSC Adv.* **2** 4632–5

[22] Wang W, Li Y, Cheng L, Cao Z and Liu W 2014 Water-soluble and phosphorus-containing carbon dots with strong green fluorescence for cell labeling *J. Mater. Chem. B* **2** 46–8

[23] Jaiswal A, Ghosh S S and Chattopadhyay A 2012 One step synthesis of C-dots by microwave mediated caramelization of poly(ethylene glycol) *Chem. Commun.* **48** 407–9

[24] Pan D, Zhang J, Li Z, Wu C, Yan X and Wu M 2010 Observation of pH-, solvent-, spin-, and excitation-dependent blue photoluminescence from carbon nanoparticles *Chem. Commun.* **46** 3681–3

[25] Zhou J, Yang Y and Zhang C-Y 2013 A low-temperature solid-phase method to synthesize highly fluorescent carbon nitride dots with tunable emission *Chem. Commun.* **49** 8605–7

[26] Zhu S J, Meng Q N, Wang L, Zhang J H, Song Y B, Jin H, Zhang K, Sun H C, Wang H Y and Yang B 2013 Highly photoluminescent carbon dots for multicolor patterning, sensors, and bioimaging *Angew. Chem. Int. Edn.* **52** 3953–7

[27] Liu C J, Zhang P, Tian F, Li W C, Li F and Liu W G 2011 One-step synthesis of surface passivated carbon nanodots by microwave assisted pyrolysis for enhanced multicolor

photoluminescence and bioimaging *J. Mater. Chem.* **21** 13163–7

[28] Sadhukhan M, Bhowmik T, Kundu M K and Barman S 2014 Facile synthesis of carbon quantum dots and thin graphene sheets for non-enzymatic sensing of hydrogen peroxide *RSC Adv.* **4** 4998–5005

[29] Lai C W, Hsiao Y H, Peng Y K and Chou P T 2012 Facile synthesis of highly emissive carbon dots from pyrolysis of glycerol; gram scale production of carbon dots/mSiO$_2$ for cell imaging and drug release *J. Mater. Chem.* **22** 14403–9

[30] Bourlinos A B, Stassinopoulos A, Anglos D, Zboril R, Karakassides M and Giannelis E P 2008 Surface functionalized carbogenic quantum dots *Small* **4** 455–8

[31] Eda G, Lin Y Y, Mattevi C, Yamaguchi H, Chen H, Chen I S, Chen C and Chhowalla M 2010 Blue photoluminescence from chemically derived graphene oxide *Adv.Mater.* **22** 505–9

[32] Ayala P, Arenal R, Loiseau A, Rubio A and Pichler T 2010 The physical and chemical properties of heteronanotubes *Rev.Mod.Phys.* 1843–5